Full Length Article

Combination of iodine-deficient BiOI phases in the presence of CNT to enhance photocatalytic activity towards phenol decomposition under visible light

Nikita Sharma [a,b], Zsolt Pap [a,c,d,*], István Székely [c,e], Monica Focsan [c], Gábor Karacs [f], Zoltan Nemeth [b], Seema Garg [g], Klara Hernadi [a,h,*]

[a] Department of Applied and Environmental Chemistry, University of Szeged, H–6720 Rerrich Béla 1, Szeged, Hungary
[b] Advanced Materials and Intelligent Technologies Higher Education and Industrial Cooperation Centre, University of Miskolc, H-3515 Miskolc, Hungary
[c] Nanostructured Materials and Bio-Nano-Interfaces Centre, Institute for Interdisciplinary Research on Bio-Nano-Sciences, Babeş–Bolyai University, RO-400271, Treboniu Laurian 42, Cluj-Napoca, Romania
[d] Institute of Research-Development-Innovation in Applied Natural Sciences, "Babeş-Bolyai" University, Fântânele 30, RO-400294, Cluj-Napoca, Romania
[e] Faculty of Physics, Babeş–Bolyai University, M. Kogălniceanu 1, 400084 Cluj–Napoca, Romania
[f] MTA-ME Materials Science Research Group, ELKH, H-3515 Miskolc-Egyetemváros, Hungary
[g] Department of Chemistry, Amity Institute of Applied Sciences, Amity University, Sector-125, Noida, U.P. 201313, India
[h] Institute of Physical Metallurgy, Metal Forming and Nanotechnology, University of Miskolc, HU-3515 Miskolc-Egyetemváros, C/1 108, Miskolc, Hungary

ARTICLE INFO

ABSTRACT

In this work, we have prepared BiOI/CNT composites by hydrothermal method and studied the impact of CNT and hydrothermal treatment conditions (temperature and time) simultaneously on phenomena such as crystallization. The samples were studied using X-ray Diffraction (XRD), nitrogen sorption (Brunauer–Emmett–Teller (BET) specific surface areas), Scanning Electron Microscopy assisted with Energy Dispersive X-Ray spectroscopy (SEM-EDX), High Resolution Transmission Electron Microscopy (HRTEM), UV–vis Diffuse Reflectance spectroscopy (DRS), Raman spectroscopy and photoluminescence spectroscopy (PL). The different heat treatments applied and varied amount of CNT was found to have a profound effect on the structural, morphological, compositional and optical properties of the prepared composites. The distinguishable changes in the above-mentioned properties were clearly visible for the samples prepared at higher temperature and longer duration (150 °C, 6.30 h). Surprisingly, the presence of other phases of BiOI, such as $Bi_7O_9I_3$, $Bi_4O_5I_2$, Bi_5O_7I, also co-existed at the same time, although in low amount. Finally, for the study, the photocatalytic efficiency of the prepared samples was tested for phenol and RhB, as model pollutants, under visible light irradiation for 240 min and 120 min, respectively. The results revealed that the composites prepared at higher temperature with longer duration showed superior performance for the photodegradation of phenol and RhB. Additionally, the composites performed better than their respective reference samples in each case. Interestingly, the introduction of CNT promoted the crystallinity in the composites and promising results for the removal of phenol and RhB were achieved by the use of low power ordinary visible lamps.

1. Introduction

Photocatalysis is considered as one of the "green technology" in the areas of environmental remediation such as in air sterilization, removal of pollutants and inactivation of microorganisms like viruses from wastewater [1]. Lately, bismuth oxyhalides (BiOX) have emerged as a new class of non-titania photocatalysts in the field of heterogeneous photocatalysis. These are popularly known for its visible light photocatalytic response, primarily, due to their narrow band gap and the electronic structure of Bi [2]. As a thumb rule, the photocatalytic activity is affected with the positions of valence band (VB) and conduction band (CB) of the photocatalyst besides the mobility of charge carriers. In case of Bi-based semiconductor photocatalyst, hybridized O 2p and Bi 6 s valence bands are present, unlike other metal oxides which consists of

only O 2*p* orbitals. The presence of this largely dispersed Bi 6 *s* orbital is beneficial for increasing the mobility of photogenerated charge carriers and reducing the band gap, as broader valence bands enhance the charge transportation. Besides this, their unique layered structure also plays an important role in effective charge separation.

BiOI, as compared to other members of BiOX family, has the lowest band gap energy ∼ 1.6–1.9 eV and crystallizes into tetragonal matlockite structure. It consist of layers of $[Bi_2O_2]^{2+}$ slabs interleaved by double slabs of negatively charged halogen atoms. BiOI has been synthesized with different morphologies from two-dimensional nanoplates or nanosheets to three-dimensional microflowers. The photocatalytic degradation of pollutants by BiOI included Rhodamine B (RhB) [3], Methyl Orange (MO) [4], Methylene Blue (MB) [5], caffeic acid [6], gallic acid [7], phenol [8,9], bisphenol-A [10] and reduction of Cr (VI) to Cr (III) [11] etc. This shows a huge tendency of BiOI in the field of photocatalysis for waste water treatment [8]. Apart from its higher photocatalytic response, in some cases, BiOI nanocomposites such as with graphene has shown higher adsorption capacity for dyes [12]. However, it still suffers from low photocatalytic efficiency when it comes to practical applications. This is mainly due to the high valence band position which lowers its photo-oxidation ability and promotes fast recombination of photo-generated charge carriers [13,14,15]. Efforts have been made to improve its visible light response, such as facet-controlled synthesis of BiOI [16], morphology-controlled synthesis [17], modifications using metals [18], non-metals (activated carbon, graphene oxide, carbon nanotube) [13] or noble elements (Au, Ag, Pt) [19]. The modifications with several carbon nanostructures including g-C_3N_4 and carbon dots are also being employed for increasing the efficiency of photocatalytic processes [20212223]. All of these works resulted in higher photon absorption ability and hindered the e^-/h^+ recombination.

In order to elevate its photocatalytic response under visible light region, strategies like composites formation or heterojunctions have been adopted resulting in the efficient separation of electron–hole pairs [24,25]. Moreover, it has a great potential for tuning the desired electronic structure and properties of composites. The most common synthesis methods used for the preparation of BiOI and its composites includes hydrothermal [26], solvothermal [27,28] and precipitation [29], out of which, hydrothermal synthesis is the most widely used. J F Florez-Rios *et al.* reported the hydrothermal synthesis of BiOI and studied the photodegradation of methyl orange dye as model pollutant under visible and UV light source. They found that BiOI powders exhibited better photocatalytic activity under visible light than in UV light. Subsequently, other oxide forms of BiOI were also discovered later, such as, $Bi_4O_5I_2$, Bi_5O_7I, $Bi_7O_9I_3$, α, β- Bi_2O_3. The thermal treatment of BiOI, unlike other bismuth oxyhalides, result in deficiency of iodine atoms, possibly, due to easy loss of iodine and subsequently, producing iodine-deficient BiOI. These BiOI oxide forms and its composite were reported to exhibit higher photoactivity than pristine BiOI [30]. Their applications include photocatalysis, photovoltaic applications [31,32,33], photoelectrochemical devices [34], H_2 production [35], X-ray detectors [36] and in antifouling activity [37].

A huge amount of research is focused on enhancing the degradation efficiency of the photocatalysts. However, less attention is paid to investigate the thorough study on the roles of modifiers, such as carbonaceous materials, and hence, explaining their influence on certain important phenomena, such as crystallization. One such commonly used modifier is carbon nanotubes which has been widely studied in the diverse field of research including material science, electrochemistry, applied physics, polymer science and environmental sciences. This is evident by the unceasing growth in number of publications concerning CNT in different areas, over the years.

Nearly all of them has focused on two common roles of CNT during photodegradation of organic pollutants. Firstly, the role as a charge separator, where it acts as an electron sink capturing the photogenerated electrons and therefore, extending the lifespan of electron and hole pairs

[38]. In this way the recombination of charge carriers is prevented which leads to an increased photocatalytic activity [39,40,41]. Secondly, it acts as a support material in most cases, especially in a photocatalyst-composite system, because of its large surface area [42]. However, there could be many other roles played by CNTs that needs investigation, such as induced band-gap shifting, crystal orientation, degree of crystallinity, and light absorption properties etc. which has a direct or indirect impact on the photocatalytic activity, also evident from our previous work with BiOBr and CNT composites [43]. Nonetheless, the amount of CNT is also a governing factor in many cases [44,45]. Some of the studies reported optimum loading amount of CNT that results in enhanced activity while higher amount of CNT marked a decrease in photocatalytic activity due to the light absorption by CNT that becomes prevalent [46].

In this work, we have synthesized composites of bismuth oxoiodides with carbon nanotubes pointing out the role of carbon nanotubes in a composite formation and its influence on the photocatalytic activity. The samples were prepared *via* hydrothermal method with varying amount of CNTs to examine their photocatalytic efficiency by studying the photocatalytic degradation of phenol and RhB under visible light.

2. Experimental

2.1. Chemicals and reagents

Bismuth nitrate pentahydrate [Bi $(NO_3)_3 \cdot 5H_2O$] (Sigma–Aldrich, 98.0%), glacial acetic acid (Molar Chemicals Ltd., 100%), potassium iodide (Molar Chemicals, 99.7 %), functionalized carbon nanotubes (Nanothinx S.A., Greece), Phenol (VWR extra pure, 100%) and RhB (Alfa Aesar, no purity data given). All the reagents were of analytical grade and used without further purification. Deionized water was used for the entire study. Methanol of HPPLC-grade was used for HPLC measurements.

2.2. Preparation of BiOI and BiOI/CNT composites

In this work, 12 samples of BiOI/CNT composites were prepared *via* hydrothermal crystallization applying different synthesis parameters, such as time and temperature of the hydrothermal crystallization, and the carbon nanotube content. For each set of synthesis conditions, 4 reference samples were also prepared without CNT. In the synthesis process, two solutions A and B were prepared. For solution A, 3 g Bi $(NO_3)_3 \cdot 5H_2O$ was dissolved in 3 mL glacial acetic acid under continuous magnetic stirring and heated up to 45 °C to speed up the mixing process until a clear transparent solution was obtained. Furthermore, a calculated amount of CNT was added based on the pre-defined composition values (0.5, 1, 2 wt%) followed by 25 mL deionized water. The mixture was sonicated for 1 h to obtain a black-coloured suspension and this was called solution A. For solution B, 1.03 g potassium iodide (KI) was dissolved in 25 mL deionized water. Solution B was added dropwise to solution A under continuous magnetic stirring and followed by 20 min of homogenization. The colour of the solution changed from yellowish to dark green and finally a brick red coloured precipitate was formed at the end of 20 min. The mixture was transferred to 120 mL Teflon®-lined stainless-steel autoclave and subjected to heat treatment at different temperature and time intervals (120 °C & 150 °C for 4:30 h and 6:30 h each). It was allowed to cool down at room temperature and the product was collected and washed with ethanol and deionized water, three times, each time using centrifugation at 4400 rpm for 5 min. The final product was dried at 60–80 °C in a vacuum furnace overnight. The Table 1 shows the list of samples prepared and following terminology has been used throughout this study.

2.3. Characterisation

The products were characterized by X-Ray Diffraction (XRD) using a

Table 1

List of BiOI and BiOI/CNT composite samples prepared at different synthesis conditions.

List of the as-prepared samples with different CNT amount and at different synthesis temperature and time conditions	
BiOI_120°C_4.30 h	BiOI_150°C_4.30 h
BiOI + 0.5 %CNT_120°C_4.30 h	BiOI + 0.5 %CNT_150°C_4.30 h
BiOI + 1 %CNT_120°C_4.30 h	BiOI + 1 %CNT_150°C_4.30 h
BiOI + 2 %CNT_120°C_4.30 h	BiOI + 2 %CNT_150°C_4.30 h
BiOI_120°C_6.30 h	BiOI_150°C_6.30 h
BiOI + 0.5 %CNT_120°C_6.30 h	BiOI + 0.5 %CNT_150°C_6.30 h
BiOI + 1 %CNT_120°C_6.30 h	BiOI + 1 %CNT_150°C_6.30 h
BiOI + 2 %CNT_120°C_6.30 h	BiOI + 2 %CNT_150°C_6.30 h

Rigaku Miniflex II diffractometer ($2\theta° = 10–70°$, λ (CuK_α) = 0.15418 nm) equipped with a graphite monochromator for the analysis of the crystal phase and structural properties of the prepared composites, such as the degree of crystallinity and crystal orientations. The mean primary crystallite size was also calculated for the samples using the Scherrer equation [47]. N_2 adsorption–desorption measurements were carried out to measure the specific surface areas of the samples, according to the BET (Brunauer-Emmett-Teller) method. Morphological and elemental compositional analysis were carried out using Scanning Electron Microscopy (SEM) with energy-dispersive X-ray (EDX) spectrometer and Transmission Electron Microscopy (TEM). For TEM measurements, the as-prepared samples were examined by high-resolution transmission electron microscopy (HRTEM, FEI Technai G2 electron microscope, 200 kV) to explore the morphology and particle size of the nanocomposites. Sample preparation was made by dropping an aqueous suspension of the nanocomposites on 300 mesh copper grids (lacey carbon, Ted Pella Inc.). The diameters of the nanoparticles were measured on the HRTEM images based on the original scale bar using ImageJ software. The optical property was analyzed using Diffuse Reflectance Spectroscopy (UV–vis-DRS) JASCO-V650 with an integration sphere (ILV-724) ($\lambda = 300–800$ nm). The indirect band-gap energy was calculated using the Kubelka-Munk equation, that is [F(R).hν] p = A(hν – E_g), where, h is Planck constant, E_g is the band gap energy, A is constant and p is dependent on the type of optical transition and is obtained by plotting the graph between $(\alpha h\nu)^{1/2}$ vs. photon energy (hν). Raman spectroscopy was used to study the composite formation and crystal defects in the prepared composites. A multilaser confocal Renishaw in Via Reflex Raman spectrometer equipped with a RenCam CCD detector was employed to record the Raman spectra. The 532 nm (green) laser was applied as an excitation source. Using a 0.9NA objective of 100 $\times$ magnification, the Raman spectra were collected. The integration times were 20 s, 1800 lines/mm grating for all spectra, and 10% of the maximum laser intensity – laser power was 20 mW. 4 cm^{-1} was the spectral resolution. The photoluminescence (PL) spectra of the materials were acquired on a fluorescence spectrophotometer (JASCO LP-6500 spectrofluorometer) with 1 nm spectral resolution equipped with Xe lamp as the excitation source and coupled to an epifluorescence accessory (EFA 383 module). The measurements were recorded in the wavelength range of 350–800 nm with fixed excitation wavelength at 365 and 450 nm.

2.4. Photocatalytic measurements

The photocatalytic activity of the composites was determined by measuring the degradation of phenol and rhodamine B in an aqueous solution under visible light. In this test, 4 $\times$ 24 W visible light lamps (irradiation time = 4:00 h) were used as visible light source. The photoreactor system was equipped with a thermostat containing 1 M sodium nitrite solution to eliminate UV light and thus prevent variation in the results. The suspension of the pollutant and photocatalyst was continuously purged with air to keep the dissolved oxygen concentration constant during the whole experiment. The initial concentration of phenol (C_0) used for the study was 0.1 mM while for RhB was 0.02 mM.

The amount of catalyst loaded was 1.0 g $\cdot$ L^{-1} with 130 mL total volume of the suspension (V_{susp}). The suspension was ultra-sonicated for 5 min. For phenol, the suspension was kept in dark for 30 min to ensure the establishment of adsorption–desorption equilibrium with continuous stirring and air supply with irradiation time of 240 min. However, in case of RhB, 60 min of dark period was used and the photocatalytic decomposition was carried out for 120 min. The samples were collected at different time intervals in both case of pollutants. The samples collected were then centrifuged for 3 min at 15000 rpm and filtered using Filtratech 0.25 μm syringe filter. The decrease in concentration of the model pollutants (phenol and RhB) were measured by HPLC and UV spectrophotometer, respectively. HPLC Merck-Hitachi L-7100 with a low-pressure gradient pump, equipped with a Merck-Hitachi L-4250 UV–Vis detector and a Lichrospher R_p 18 column using a methanol/water (50:50 v/v) mixture as eluent was used for measurements. The detection wavelength for RhB was 553 nm and for phenol 210 nm.

3. Results and discussions

3.1. X-Ray diffraction (XRD)

In the first instance, the diffraction patterns of the as-prepared BiOI/CNT composites and their appropriate references was investigated. The presence of pure BiOI and the coexistence of different iodine-deficient BiOI phases was detected. Phases such as $Bi_4O_5I_2$, $Bi_7O_9I_3$ and Bi_5O_7I were observed. Fig. 1 (a) and (b) shows the diffraction pattern of the sample series prepared at 150 °C at 6.30 and 4.30 h, respectively. The characteristic peaks for CNT was not observed due to their relatively low amount.

It is interesting to note that all the characteristic peaks for BiOI tetragonal phase (JCPDS 00–73-2062, 10–0445) were shifted to smaller diffraction angles (shown in Fig. 1 (c)). For instance, the characteristic peak for the most intense peak (1 0 2) plane of BiOI was shifted from 29.7° to 28.6°-28.8° (Fig. 1 (c)). This shifting was observed in nearly all the samples. The peaks found at 28.6° and 28.8° corresponds to the characteristic peak of $Bi_7O_9I_3$ and $Bi_4O_5I_2$, respectively, also reported previously[14,15]. This shifting of peaks is probably due to the extra bismuth and oxygen atoms in BiOI crystal lattice which is well-supported by other reports giving rise to other iodine-deficient bismuth oxoiodides[48]. The diffraction pattern of $Bi_4O_5I_2$ (characteristic peak at 28.8° JCSD-713448) is quite different from that of BiOI (characteristic peak at 29.7°, JCPDS no.–10–0445), which makes it easier to distinguish between these two phases. Interestingly, it has been reported that the diffractogram of tetragonal BiOI and $Bi_7O_9I_3$ are very similar and hard to identify the two phases [26]. We can say that this statement seems to be misleading since after a thorough literature reading we found that the standard JCPDS file of $Bi_7O_9I_3$ diffraction pattern is wrongly quoted everywhere and rather, in most cases, denoted to $Bi_4O_5I_2$-based studies. Therefore, we concluded that the diffraction patterns of $Bi_4O_5I_2$ and $Bi_7O_9I_3$ are very close to each other with their characteristic peaks at 28.8° and 28.6°. This is because the more the iodine loss, the stronger the shift of diffraction peaks to lower angle is observed due to increase in lattice parameters [49].

Through XRD results it seems that the presence of $Bi_4O_5I_2$ is observed in the case of samples prepared at higher temperature (150 °C) while lower temperature leads to stabilisation of $Bi_7O_9I_3$ and Bi_5O_7I phases. This phase transformation process in BiOI is supported by the fact that as the heat treatment is applied or calcination of BiOI is progressed, pure BiOI transforms to other oxide forms since those are thermodynamically favourable [50]. Yu. Changlin *et al.* also reported about the thermal instability of BiOI [51]. Unlike reported in their work about the lower temperature conditions influencing the crystallinity of the samples, in our case, CNTs enhanced the crystallinity of our samples which was also observed in our previous work [43]. With increasing amount of CNT, higher degree of crystallization was observed which, indeed, influences the photodegradation efficiency. In this way, it could be said that CNT
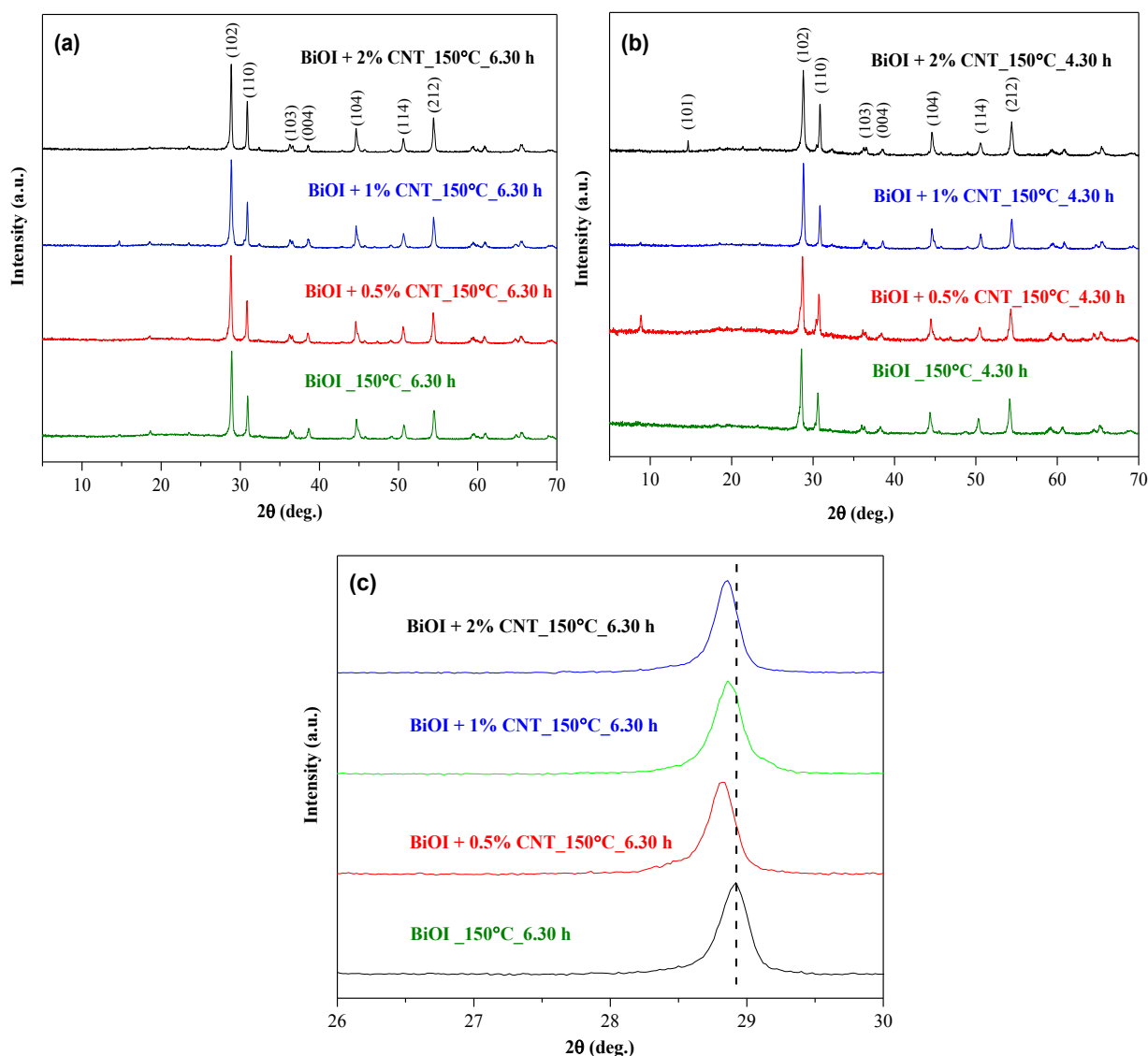
Fig. 1. XRD diffractograms of BiOI and BiOI/CNT sample series belonging to the higher temperature conditions prepared at different time intervals (a) 150 °C at 6.30 h (b) 150 °C at 4.30 h (c) expanded XRD diffraction patterns of the BiOI/CNT samples fabricated at 150 °C for 6.30 h.

favours ordered structure. Hence, for obtaining crystalline structures, CNT could play a significant role. Finally, the primary crystallite size of all the samples were calculated *via* Scherrer Equation and fall in the range between 55 nm and 90 nm, except for the sample "BiOI_120°C_4.30 h". Moreover, the variations in crystallite size were found to be independent of the amount of CNTs. There is also no significant difference observed in the particle size based on different synthesis conditions. On whole, the effect of synthesis conditions on the occurrence of different forms of bismuth oxoiodides are following:

(i) Applying higher temperature conditions for longer duration (150 °C, 6.30 h), $Bi_4O_5I_2$ phase was identified.
(ii) When the temperature was increased but with shorter duration (150 °C, 4.30 h), $Bi_4O_5I_2$ phase became prominent again.
(iii) When the temperature was decreased (at 120 °C), irrespective of time, the end result indicated the presence of different phases ($Bi_7O_9I_3$ + Bi_5O_7I). In a similar condition, the presence of mixed phases was observed and such changes were stated due to the difference in pH conditions, as reported by Xian Xao *et al.* [52].

These results suggest that the heat-treatment process plays a very

crucial role in defining the conversion and formation of new crystal structures, also highlighted by Hang Liu [53]. Herein, correctly identifying the different phases of BiOI becomes very important as will be discussed in the subsequent sections. As we know, high temperature treatment of BiOI such as annealing or calcination results in phase transformation of BiOI. However, in our study, phase transformation of BiOI occurred at lower temperature conditions. This subject, therefore, raises question on the stability of BiOI formation even at lower synthesis temperature conditions. If the above descriptions are true about the presence of iodine-deficiency species then we may get some confirmation through the following section of EDX (Section 3.2).

3.2. Energy dispersive X-Ray analysis (EDX)

The samples were tested for their elemental composition by EDX spectrometer. As demonstrated in the previous sections of XRD, the higher temperature condition led to changes in structural property of the composites. Interestingly, similar observations were also seen in case of compositional characteristics. The EDX measurement of samples synthesised at 150 °C showed the compositional changes which indicated the iodine-deficiency, as presented in Table 2. Further, the iodine

Table 2
Atomic ratio values of Bi/I/O elements in sample series of BiOI and BiOI/CNT prepared at 150 °C and 4.30 h.

Sample	Bi (atomic%)	I% (atomic%)	O% (atomic%)	Theoretical Ratio (Bi:I:O)	Experimental Ratio (Bi:I:O)
BiOI_150°C _4.30 h	15.44	14.48	66.39	1:1:1	1:0.93:4.30
BiOI + 0.5 %CNT_150°C _4.30 h	16.47	14.49	64.51	1:1:1	1:0.88:3.92
BiOI + 1 %CNT_150°C _4.30 h	16.37	15.12	64.00	1:1:1	1:0.92:3.91
BiOI + 2 %CNT_150°C _4.30 h	17.43	14.53	65.41	1:1:1	1:0.83:3.75

leaching was also observed during washing of samples which again indicates the loss of iodine from the samples. Not only this but iodine fumes were also visible when autoclaves were opened at the end of synthesis process and the "free" iodine painted the Teflon of the autoclave in "pinkish/purplish" colour that again proves iodine deficiency in the prepared samples. At this point, it is important to note that iodine was not added in excess (see synthesis section). The EDX spectrum demonstrated the presence of main elements of the composites (Bi, O and I). EDX spectra of a sample can be found in Fig S1 (Supporting file).

This loss of iodide atoms could be considered as defects which, in turn, are known for enhancing the photocatalytic response. The defects could act as active centre at the interface between catalyst and organic pollutant surface. For instance, Montero et al has reported a direct connection between the photocatalytic activity and defects type indicating that they play an important role in altering the photocatalytic response [54]. In several other cases it could be seen that presence of defects extended the light absorption spectral range of many photocatalysts, including ZnO and TiO$_2$ [55,56].

3.3. Scanning electron microscopy (SEM) and high resolution Transmission electron microscopy (TEM)

The morphology of the composites was analysed by SEM. As shown in Fig. 2, clearly two distinct types of morphologies were observed with changes in the hydrothermal crystallization temperature conditions. With rise in temperature from 120 °C to 150 °C, a complete transformation in morphology was observed, from sheet-like to microflower-type morphology, respectively. The prepared composites have irregular nanosheet-like morphology with smooth surface at 120 °C, as shown in Fig. 2 (a-c). The catalyst particles could be seen as aggregated on the CNT's surface. CNT were found to be non-uniformly distributed throughout the sample. Also, the nanosheets were stacked on top of each other and partially aggregated as well (Fig. 2 (a)). Apart from agglomeration of nanosheets and carbon nanotubes, there were holes present on

the surface of microsheets obtained at lower temperature conditions (120 °C). Similar porous-kind of morphology was also observed by Yang et al, where they synthesized porous Bi$_5$O$_7$I nanosheets [57]. At higher temperature (150 °C), microflower-like morphology was found. Fig. 2 shows the deposition of catalyst particles on the walls of CNT. In most of the studies, it was reported that the use of solvents like polyethylene glycol [58] can facilitate in obtaining hierarchal structures and helps in the prevention of agglomeration of sheets but the use of water doesn't seems to solve this problem. However, in our study, no organic solvent was used throughout the study, rather change in temperature conditions led to a three-dimensional morphology. It could be said that the self-assembly of sheets occurred at higher temperature conditions without the use of surfactants or any template-directing agents.

The morphology of MWCNT-based composite materials was investigated by HRTEM technique. Fig. 3 a-d shows TEM micrographs of BiOI (Fig. 3 a), and BiOI/CNT (Fig. 3 b-d) nanocomposites at various CNT content, respectively. From TEM images, it can be concluded that larger BiOI inorganic microparticles are attached to the surface of CNTs. Based on detailed electron microscopy investigation, no significant difference was found between the morphologies of nanocomposites produced with various CNT contents. We also took into consideration that the TEM images show only a two-dimensional projection of the real three-dimensional particles; consequently, the observed particle size distribution is practically a distribution of the projected dimension of the particles. Based on the TEM observations the average particle size of the BiOI particles was approximately 1 μm which showed good agreement with the measured particles size values originating from XRD and SEM investigations.

3.4. N$_2$ Adsorption

All the samples prepared were found to have low specific surface area ranging from 2.6 to 9.2 m^2/g. However, no specific trends were observed with different CNT content or hydrothermal synthesis
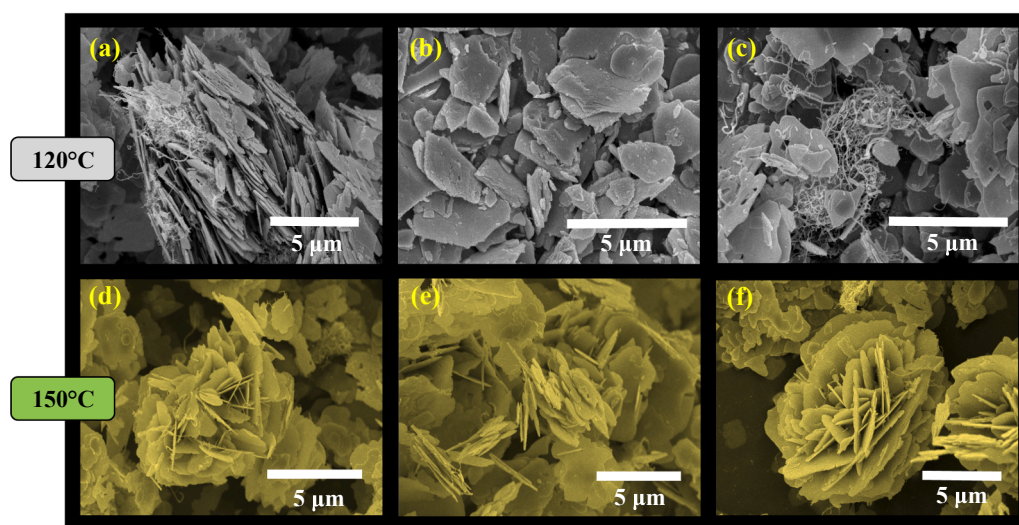

Fig. 2. SEM micrographs of BiOI and BiOI/CNT composites prepared at 120 °C and 150 °C (a) BiOI + 1 %CNT_120°C_6.30 h (b) BiOI_120°C_4.30 h (c) BiOI + 1 % CNT_120°C_4.30 h (d, e) BiOI + 1 %CNT_150°C_6.30 h (f) BiOI + 0.5 %CNT_150°C_4.30 h.
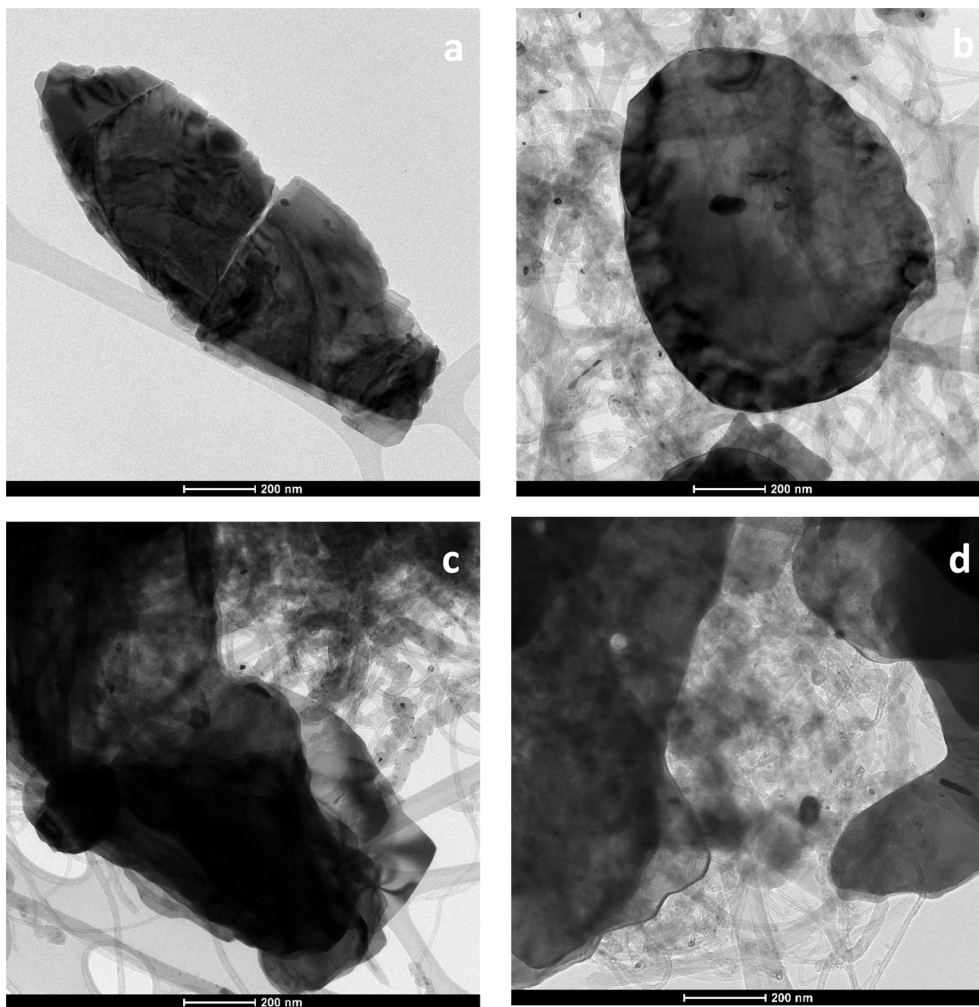
Fig. 3. Representative TEM micrographs of BiOI (a); BiOI + 0.5% CNT (b); BiOI + 1% CNT (c) and BiOI + 2% CNT nanocomposites (d) prepared at 150C and 6.30 h.

conditions (time and temperature). The low specific surface area of composites is also evident from XRD which is the higher primary crystallite size of the prepared samples. As discussed, the samples have low

specific surface areas which was also reported in a study by Yun Jang et al. [57]. These low values for specific surface area of our samples is usual in case of bismuth-based semiconductors such as bismuth
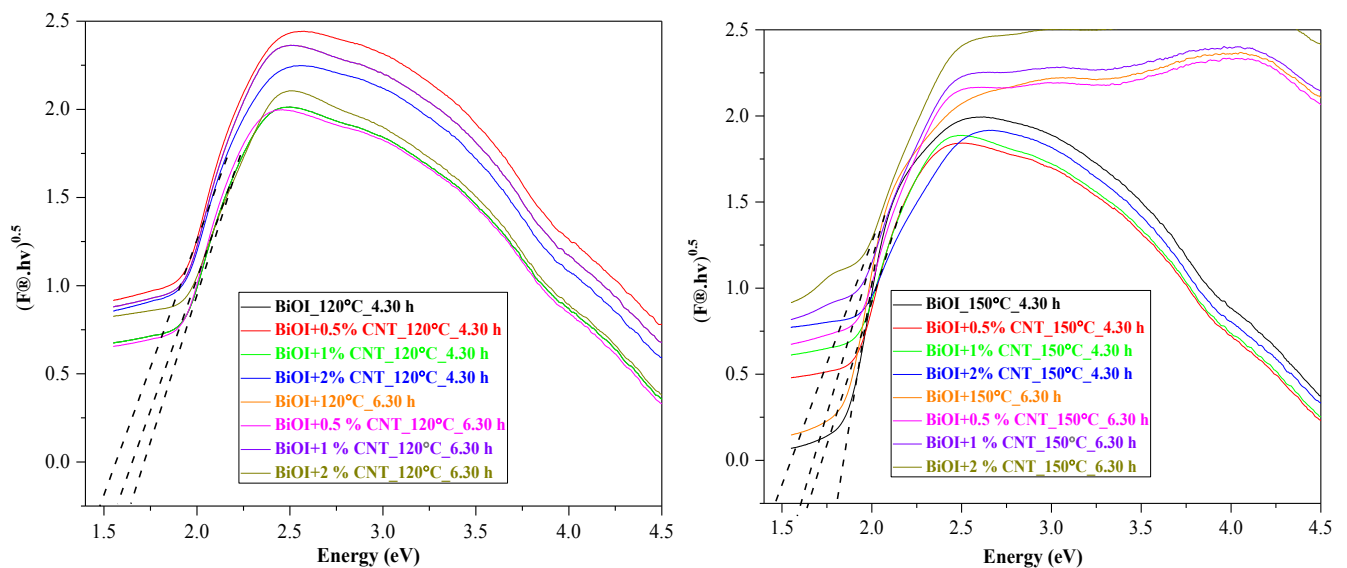
Fig. 4. UV–Vis DRS plots of transformed Kubelka-Munk function versus the energy of sample series at low and high temperature conditions with different CNT% (a) BiOI and BiOI/CNT at 120 °C at 4.30 h (b) BiOI and BiOI/CNT at 150 °C at 6.30 h.

oxoiodides [59]. The specific surface area of the sample BiOI + 2 % CNT_150_6.30 h was calculated to be 6.7 m^2/g which is 2.6 times of its reference sample.

3.5. Optical measurements

The optical properties of the composites were investigated by UV–Vis diffuse reflectance spectroscopy (UV-DRS). Fig. 4 (a) and (b) shows the DRS spectra of the composites for the band gap values of the prepared samples. The light absorption edge of the composites was above 620 nm which suggests that the composites can be efficiently excited under visible light. The E_g of the prepared samples fall in the range of 1.46 – 1.82 eV. In the case of the samples prepared at lower temperature condition (120 °C) with nanosheets morphology, E_g values was in the range between 1.60 and 1.79 eV while in the case of higher temperature (150 °C) with microflower-like morphology, the broader range of E_g was observed ranging from 1.46 to 1.82 eV. The blue shift in absorption edge maximum was observed. This blue shift is probably due to several iodine deficiency or defects created by iodine deficiency which modifies the band structure, also reported by Xuewen Wang et al. [34]. This is in accordance with a report where a similar shift was noticed in samples with iodine deficiency and oxygen rich bismuth oxoiodides.

Clearly, the transition from tetragonal BiOI to monoclinic $Bi_4O_5I_2$ occurred when temperature was raised from 120 °C to 150 °C. As evident from our XRD and EDX discussions (Sections 3.1. and 3.2.) about the successful identification of iodine-deficient BiOI ($Bi_4O_5I_2$ + $Bi_7O_9I_3$ + Bi_5O_7I), this could be further supported through our DRS results which indicates the presence of compounds in a stoichiometric ratio. This means that if there is presence of non-stoichiometric compounds then their peaks of first derivative spectra would be randomly distributed which in contrast to our results, lies on the same point.

Another spectacular observation found was the relation of iodine deficiency on band gap values of composites. Theoretically, $Bi_4O_5I_2$ has least iodine deficiency and those samples containing predominantly $Bi_4O_5I_2$ phase showed lower band gap values. In contrast, $Bi_7O_9I_3$ and Bi_5O_7I are relatively more iodine-deficient and samples with these phases attained higher band gap.

3.6. Raman measurements

The Raman spectra of the BiOI and BiOI/CNT samples reveal information about the samples' crystallinity and surface defects. We identified vibrations modes at 96, 125, 148 (weak shoulder of the 125 cm^{-1} vibration mode), 238, and 307 cm^{-1} in the Raman spectra, as shown in Fig. 5 (a). We also observed weak shoulders in the 400 – 500 and 550 – 650 cm^{-1} regions. The Raman bands at 96 (slightly cut off on the spectrum), 125 and 148 cm^{-1} correspond to the Bi-X, respectively Bi-I bonds [60–62]. The band at 238 and 307 cm^{-1} correspond to Bi-O vibrations bonds [63,64]. The shoulders in the 400 – 500 and 550 – 650 cm^{-1} regions have been attributed to the Bi-O and Bi-O-Bi bonds [60,63]. Regarding the presence of CNT in the composites, it is speculative to prove it by Raman Spectroscopy since only the G band was identified in the spectra, see Fig. 5 (b). The weak intensity of the G band and the D band's lack could be explained by the small amount of the added CNT.

From the information obtained from the Raman spectra, there is probably not only BiOI but also other bismuth oxides in the samples, evidenced by the shoulders at 238 cm^{-1}, between 400 and 500 and 550 – 650 cm^{-1} regions, and the band at 307 cm^{-1}. These bands appeared in every sample, so it is safe to conclude that the CNT addition did not induce their presence.

To prove the presence of surface defect in the samples, respectively I-vacancies, we have used the information obtained from the Raman spectra. To determine the surface defects ratio, we have chosen the intensities of the 307, 238 and 125 cm^{-1} bands since they provide information about the Bi-O and Bi-I bonds. The ratio of the following
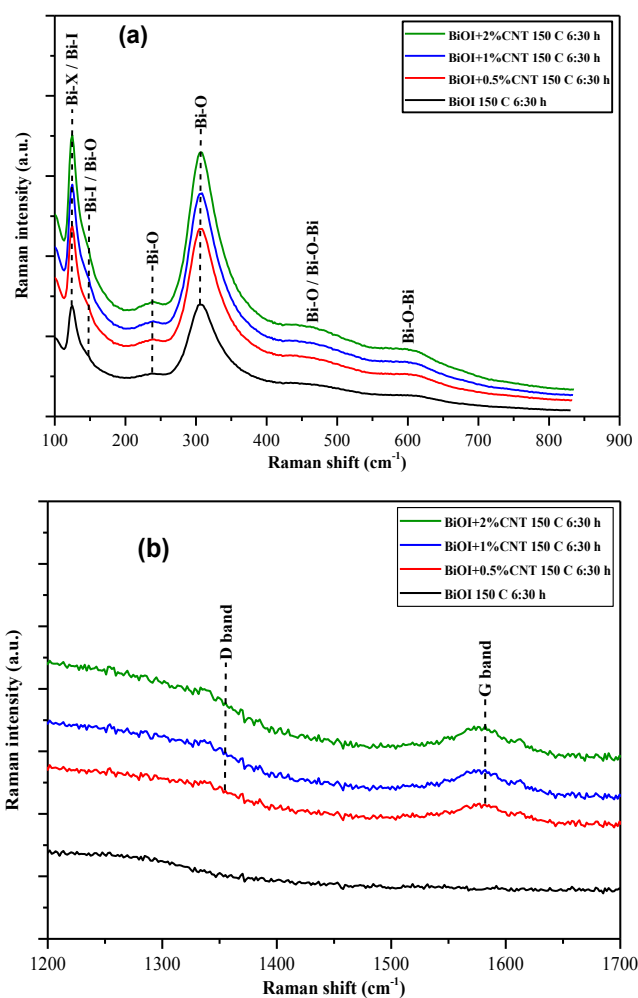

Fig. 5. **(a)** Raman spectra of BiOI and BiOI/CNT composite samples **(b)** D and G bands of the CNT.

intensities was calculated: I_{307}/I_{125}, respectively I_{238}/I_{125}. The percentage of carbon nanotubes directly influenced the samples' surface defects (Fig. 6 (a) – increased percentage of CNT lead to a higher number of surface defects, but also it impacts the photocatalytic activity concerning phenol degradation. The sample to which no CNT was added presented the smallest number of surface defects, but also the lowest photodegradation of phenol. The addition of CNT to the samples lead to more and more surface defects; which in turn lead to a higher photocatalytic activity for phenol degradation. This behaviour can be explained as with increase in the number of surface defects, more and more so-called active sites on the samples' surface are present which help to generate •OH and •O_2^- radicals, which are crucial for the photocatalytic degradation of phenol[1665].

Concerning the percentage of CNT and surface defects determined from the I_{238}/I_{125} ratio (Fig. 6 (b)) no obvious trend can be observed between them, but it should be mentioned that the peak percentage of CNT lead to the highest number of surface defects. In contrast when CNT presence was on 1% the lowest number of surface defects was observed. Just as in the case of phenol degradation, also in the case of Rhodamine B degradation the same phenomenon was observed – namely that a higher number of surface defects leads to higher conversion rates. In contrast with phenol degradation, these surface defects, in the case of Rhodamine B can act also as active sites for the adsorption of the dye, but as well can enhance the samples' photocatalytic activity – by generating •OH and •O_2^- radicals, thus improving the photocatalytic activity [66,67].
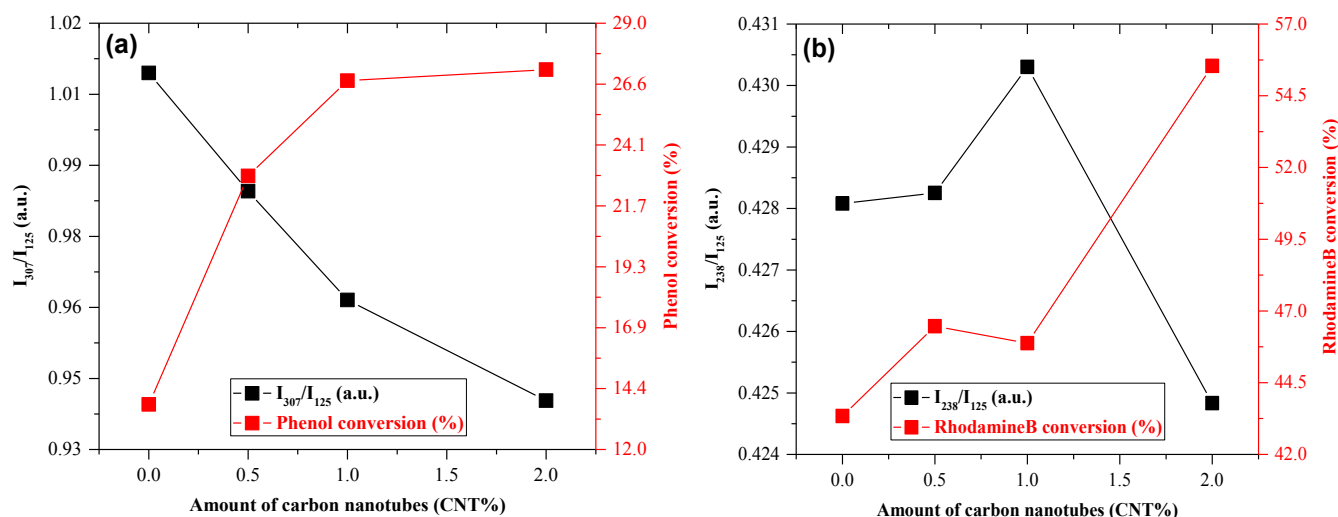
Fig. 6. Correlations between the samples surface defects and degradation efficiency in function of carbon nanotubes percentage in the samples for **(a) phenol (b) RhB.**

3.7. Photoluminescence spectra

The photoluminescence is one of the most useful technique to evaluate the recombination rate of electron/hole pairs (e^-/h^+). Fig. 7 (a) and (b) shows the PL spectra with excitation wavelengths at 450 nm and 365 nm, respectively. As we know, the lower intensity of PL spectra means lower recombination rate of e^-/h^+. In our case also, we could observe lower PL intensity and no fluorescence signal detected which indicated extremely low probability of charge carriers in all the sample cases suggesting higher photodegradation for phenol.

3.8. Photocatalytic measurements

Photocatalytic efficiency of the prepared samples was demonstrated by the removal of two model pollutants (phenol and RhB) in aqueous solution under visible light ($\lambda > 420$ nm). This time-dependence degradation efficiency of the BiOI/CNT composites was compared with their respective reference samples (without CNT), as shown in Fig. 8 (a). The composites were tested first for phenol and the minimum degradation efficiency obtained was around 13% after 240 min under

visible light irradiation. This low efficiency was observed in the case of all reference samples. Conversely, an improved photocatalytic activity was seen in the case of all composites. The highest degradation efficiency of around 28% was achieved by the composite BiOI + 0.5 % CNT_120_4.30 h followed by BiOI + 2 %CNT_150_6.30 h under visible light irradiation. The obtained-results show that in case of phenol the composites performed better than their respective references with maximum degradation efficiency of almost 2.8 times of the reference samples under visible light irradiation. Supplementary file, Fig. S2 (a) and (b) show graphs representing the photocatalytic efficiency of the samples. This can be considered among promising results since phenol has a complex degradation mechanism, which involves phenol intermediates, and the kinetics of the phenol mineralization probably consists of competitive degradation reactions between phenol and its intermediates, respectively, phenol is known to have a poor adsorption affinity. Also, ordinary lamps were used rather than expensive Xenon lamps which points towards cost-effectiveness.

The overall photocatalytic efficiency of the different sample series was also evaluated for RhB as model pollutant under visible light irradiation for a period of 120 min. Likewise for RhB, the composites with
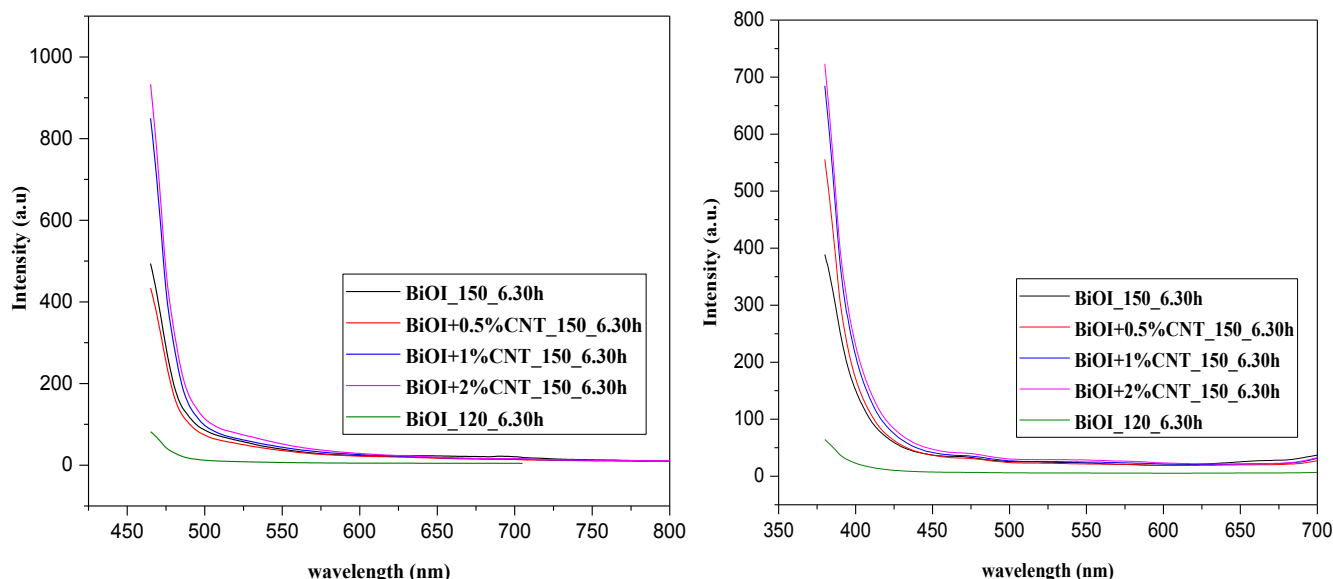

Fig. 7. Photoluminescence spectra of BiOI and BiOI/CNT composites at (a) 450 nm (b) 365 nm.
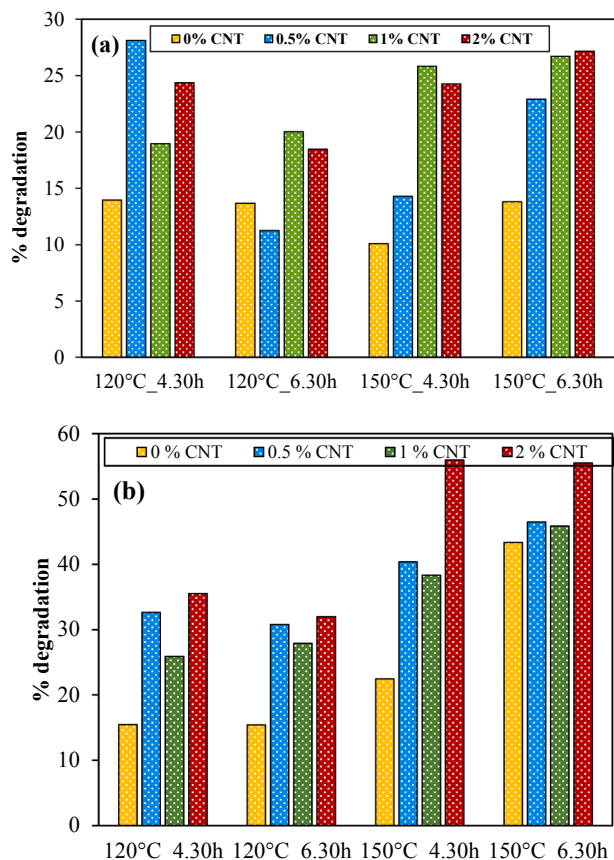
Fig. 8. (a) Degradation efficiency of composites with different %CNT for removal of phenol under visible light (b) Degradation efficiency of composites with different %CNT for removal of RhB under visible light.

Fig. 9. Correlation between the band gap energy of composites with photocatalytic degradation efficiency of (a) phenol, and (b) RhB under visible light irradiation.

CNT showed higher photocatalytic activity than their reference samples, see Fig. 8 (b). Similarly, in supplementary file, Fig. S3 (a) and (b) compare the activity response of reference samples (without CNT) and the best performing composites (whole sample series of 150°C_6.30 h). As can be seen from Fig. 8 (b), with increasing CNT content, the photocatalytic activity of these composites increased as well, with the maximum degradation efficiency of 56% under visible light irradiation. This is almost 2.5 times of its reference. It is noteworthy to point here that at this temperature the composites attained micro-flower morphology, which has been known to contribute to enhancing the rate of photodegradation process. The second-best performing sample series were also from the higher temperature series but with shorter duration, which again has micro-flower type morphology. Among all, the composite "BiOI + 2% CNT_150_4.30 h" showed the best photocatalytic activity for RhB under visible light after 120 min, as evident from the Fig. 8 (b), while the same sample also performed relatively good in case of phenol photodegradation with almost 24% degradation efficiency under visible light irradiation. Majority of the samples shows increasing trend for RhB degradation as CNT content was increasing, which again proves that CNT addition also results in gain of activity, besides imparting crystallinity in the composites structures.

The best parameter to analyze the photocatalytic activity of the semiconductor photocatalyst is their band gap (E_g). For that reason, we made some noteworthy correlations with the E_g of all the samples with their respective photocatalytic activity for phenol and RhB and then connecting with the different phase compositions, as confirmed through our XRD, EDX and DRS results above.

Firstly, the connection between E_g and photocatalytic activity of the composites were made, shown in Fig. 9 (a) and (b). The correlation shows the similar trend for band gap energies of the composites to the
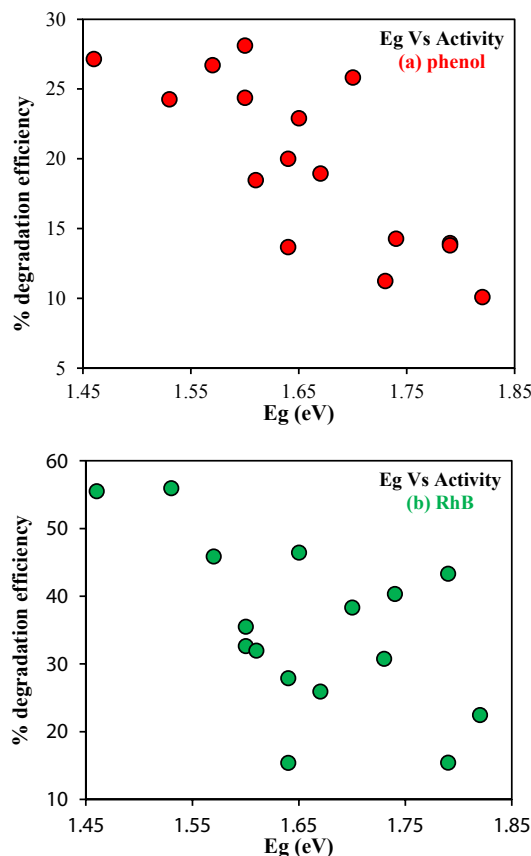
degradation efficiency for both the pollutants (phenol and RhB) under visible light. From Fig. 9, it is clear that as the band gap energy of the composites is increased, the photocatalytic activity decreases. This was an opposite trend observed as compared to our previous studies on BiOBr/CNT composites [43]. Besides, as mentioned in our DRS (Section 3.5.), the sample with dominant phase $Bi_4O_5I_2$, has lower band gap energy value. Clearly, it is now also visible from our correlation that samples with lower E_g outperforms the samples with higher band gap. Therefore, $Bi_4O_5I_2$ could be regarded as an active phase. Similarly, for samples with the presence of $Bi_7O_9I_3$ phase which is reverse in the case of samples with Bi_5O_7I phase.

Another significant correlation was made with the E_g and the presence of these different iodine-deficient BiOI species. The following observations were derived from this:

a) It can be seen from Fig. 10 that samples containing $Bi_4O_5I_2$ (denoted by number 5) is the most active, again verified previously from Fig. 9.

b) The samples with $Bi_7O_9I_3$ (denoted by number 9) have relatively moderate activity.

c) The samples with Bi_5O_7I (denoted by number 7) are the least active, even in its pure phase form, unlike the above-mentioned two phases, also justified from Fig. 9.

d) Another significant thing to be considered here is when the samples consisted of the pure phase only (numbered as 5 or 7 or 9), the activity was lower as compared to the samples comprising of mixed phases (for eg. 5 + 9 or 9 + 7 or 5 + 7).

Theoretically the order of iodine deficiency in these compounds follows the order as: $Bi_5O_7I > Bi_7O_9I_3 > Bi_4O_5I_2$, which means Bi_5O_7I
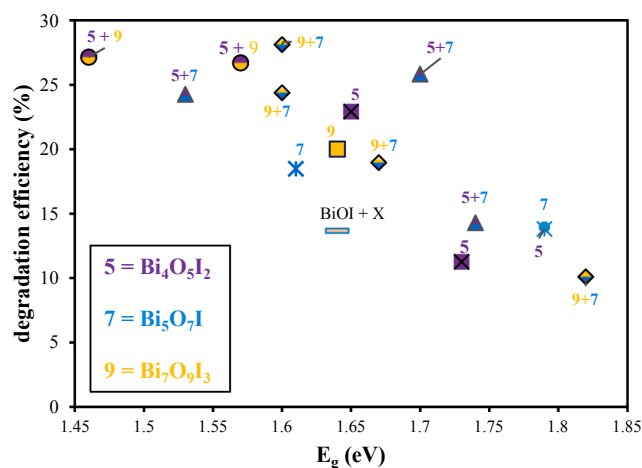
Fig. 10. Correlation with E_g, photocatalytic efficiency and different phases of iodine-deficient BiOI.

has least amount of iodine out of all and **Bi₄O₅I₂** contains maximum iodine than the rest two. After carefully analyzing the correlations given in Fig. 10, we can say that the activity of pure phases was enhanced when combined with other phases. This can be thought of appearance of a "junction" at the inner composite interfaces, in other words meaning that due to the presence of mixed phases in the sample it leads to the formation of certain heterojunctions within the structure just like in the case of TiO_2 (at the interface of anatase and rutile phase) and that could be the reason for an enhanced activity of the composites. Moreover, the presence of CNT is yet another important factor for increased photocatalytic activity, as can be seen in Fig. 9 (a) and (b). With slight increase in CNT content, high photocatalytic activity can be obtained. Therefore, it could be concluded here that a number of factors are contributing in efficient removal of the pollutants (phenol and RhB) and their interdependence can explain the significance of studying about the instable behavior of bismuth oxoiodides.

4. Conclusion

In summary, BiOI/CNT composites were synthesised at different time and temperature conditions *via* hydrothermal method. Different compositions of composites with CNT were prepared (0.5%, 1%, 2%). All three different parameters (synthesis temperature, synthesis time and CNT) have affected the prepared composites in different ways. First and foremost, noticeable changes were observed through SEM investigations in morphology indicating the transformation from nanosheets to microflower-like structures as the temperature increased. Thereafter, higher degradation efficiency for phenol and RhB was achieved by BiOI/CNT composites than their respective reference samples. Moreover, the composites with microflower morphology showed superior photocatalytic performance for both the pollutants. The results achieved for the photodegradation of phenol, in this study, are promising since ordinary visible light was used as a source of irradiation, unlike Xe-lamps which are commonly used. The different aspects reported for the enhanced photocatalytic activity of the composites are crystallinity, presence of more than one phase (iodine-deficient) in BiOI, CNT and last but not the least, the synthesis parameters. By changing the synthesis conditions, we observed that mixed phases in BiOI were present. In this way, we can say that this study provides a clear understanding of the instability of BiOI existence as pure phase even at lower temperature conditions, without using any special treatments, like annealing or calcination, which requires higher temperature conditions. At every point it is vital to identify the different type of BiOI present so as to answer adequately which phase is responsible for the photocatalytic activity enhancement.

Appendix A. Supplementary data

Supplementary data to this article can be found online at https://doi.org/10.1016/j.apsusc.2021.150605.

References

[1] A. Habibi-Yangjeh, S. Asadzadeh-Khaneghah, S. Feizpoor, A. Rouhi, Review on heterogeneous photocatalytic disinfection of waterborne, airborne, and foodborne viruses: Can we win against pathogenic viruses? J. Colloid Interface Sci. 580 (2020) 503–514, https://doi.org/10.1016/j.jcis.2020.07.047.
[2] H. AN, Y. DU, T. WANG, C. WANG, W. HAO, J. ZHANG, Photocatalytic properties of BiOX (X =Cl, Br, and I), Rare Met. 27 (3) (2008) 243–250.
[3] X. Wang, S. Yang, H. Li, W. Zhao, C. Sun, H. He, High adsorption and efficient visible-light-photodegradation for cationic Rhodamine B with microspheric BiOI photocatalyst, RSC Adv. 4 (80) (2014) 42530–42537, https://doi.org/10.1039/C4RA05506C.
[4] X. Xiao, Y. Lin, B. Pan, W. Fan, Y. Huang, Photocatalytic degradation of methyl orange by BiOI/Bi4O5I2 microspheres under visible light irradiation, Inorg. Chem. Commun. 93 (2018) 65–68, https://doi.org/10.1016/j.inoche.2018.05.009.
[5] T. Yan, H. Liu, M. Sun, X. Wang, M. Li, Q. Yan, W. Xu, B. Du, Efficient photocatalytic degradation of bisphenol A and dye pollutants over BiOI/Zn2SnO4 heterojunction photocatalyst, RSC Adv. 5 (14) (2015) 10688–10696, https://doi.org/10.1039/C4RA13990A.
[6] A.C. Mera, Y. Moreno, J.Y. Pivan, O. Peña, H.D. Mansilla, Solvothermal synthesis of BiOI microspheres: Effect of the reaction time on the morphology and photocatalytic activity, J. Photochem. Photobiol. A Chem. 289 (2014) 7–13, https://doi.org/10.1016/j.jphotochem.2014.05.015.
[7] A.C. Mera, D. Contreras, N. Escalona, H.D. Mansilla, BiOI microspheres for photocatalytic degradation of gallic acid, J. Photochem. Photobiol. A Chem. 318 (2016) 71–76, https://doi.org/10.1016/j.jphotochem.2015.12.005.
[8] Y. Li, J. Wang, H. Yao, L. Dang, Z. Li, Journal of Molecular Catalysis A : Chemical Efficient decomposition of organic compounds and reaction mechanism with BiOI photocatalyst under visible light irradiation, "Journal Mol. Catal. A, Chem. 334 (1-2) (2011) 116–122, https://doi.org/10.1016/j.molcata.2010.11.005.
[9] X. Huang, Q. Guo, B. Yan, H. Liu, K. Chen, S. Wei, Y. Wu, L.i. Wang, Study on photocatalytic degradation of phenol by BiOI/Bi2WO6 layered heterojunction synthesized by hydrothermal method, J. Mol. Liq. 322 (2021) 114965, https://doi.org/10.1016/j.molliq.2020.114965.
[10] M. Pan, H. Zhang, G. Gao, L.u. Liu, W. Chen, Facet-Dependent Catalytic Activity of Nanosheet-Assembled Bismuth Oxyiodide Microspheres in Degradation of Bisphenol A, Environ. Sci. Technol. 49 (10) (2015) 6240–6248, https://doi.org/10.1021/acs.est.5b00626.
[11] J. Jiang, Z. Mu, P. Zhao, H. Wang, Y. Lin, Photogenerated charge behavior of BiOI/g-C3N4 photocatalyst in photoreduction of Cr (VI): A novel understanding for high-

performance, Mater. Chem. Phys. 252 (2020) 123194, https://doi.org/10.1016/j.matchemphys.2020.123194.

[12] H. Liu, W.R. Cao, Y. Su, Z. Chen, Y. Wang, Bismuth oxyiodide-graphene nanocomposites with high visible light photocatalytic activity, J. Colloid Interface Sci. 398 (2013) 161–167, https://doi.org/10.1016/j.jcis.2013.02.007.

[13] J. Hou, K. Jiang, M. Shen, R. Wei, X. Wu, F. Idrees, C. Cao, Micro and nano hierachical structures of BiOI/activated carbon for efficient visible-light-photocatalytic reactions, Sci. Rep. 7 (2017) 2–11, https://doi.org/10.1038/s41598-017-12266-x.

[14] H. Liu, Y. Su, Z. Chen, Z. Jin, Y. Wang, Bi7O9I3/reduced graphene oxide composite as an efficient visible-light-driven photocatalyst for degradation of organic contaminants, J. Mol. Catal. A Chem. 391 (2014) 175–182, https://doi.org/10.1016/j.molcata.2014.04.029.

[15] J. Xia, M. Ji, J. Di, B. Wang, S. Yin, M. He, Q. Zhang, H. Li, Improved photocatalytic activity of few-layer Bi4O5I2nanosheets induced by efficient charge separation and lower valence position, J. Alloys Compd. 695 (2017) 922–930, https://doi.org/10.1016/j.jallcom.2016.10.203.

[16] S. Luo, J. Chen, Z. Huang, C. Liu, M. Fang, Controllable synthesis of Titania-Supported Bismuth Oxyiodide Heterostructured Nanofibers with Highly Exposed (1 1 0) Bismuth Oxyiodide Facets for Enhanced Photocatalytic Activity, ChemCatChem. 8 (2016) 3780–3789, https://doi.org/10.1002/cctc.201601047.

[17] C. Liao, Z. Ma, X. Chen, X. He, J. Qiu, Controlled synthesis of bismuth oxyiodide toward optimization of photocatalytic performance, Appl. Surf. Sci. 387 (2016) 1247–1256, https://doi.org/10.1016/j.apsusc.2016.06.140.

[18] F. Zhang, H. Peng, S. Jiang, C. Wang, X. Xu, L. Wang, Construction of precious metal-loaded BiOI semiconductor materials with improved photocatalytic activity for microcystin-LR degradation, Environ. Sci. Pollut. Res. 26 (8) (2019) 8226–8236, https://doi.org/10.1007/s11356-019-04266-3.

[19] X. Yu, Y. Yan, X. Yao, C. Ma, P. Huo, Y. Yan, Ag/BiOI/C enhanced photocatalytic activity under visible light irradiation, J. Dispers. Sci. Technol. 42 (8) (2021) 1116–1124, https://doi.org/10.1080/01932691.2020.1726181.

[20] S. Asadzadeh-Khaneghah, A. Habibi-Yangjeh, g-C3N4/carbon dot-based nanocomposites serve as efficacious photocatalysts for environmental purification and energy generation: A review, J. Clean. Prod. 276 (2020) 124319, https://doi.org/10.1016/j.jclepro.2020.124319.

[21] M. Singh, A. Kumar, V. Krishnan, Influence of different bismuth oxyhalides on the photocatalytic activity of graphitic carbon nitride: a comparative study under natural sunlight, Mater. Adv. 1 (5) (2020) 1262–1272, https://doi.org/10.1039/D0MA00294A.

[22] H. Che, G. Che, H. Dong, W. Hu, H. Hu, C. Liu, C. Li, Fabrication of Z-scheme Bi 3 O 4 Cl/g-C 3 N 4 2D/2D heterojunctions with enhanced interfacial charge separation and photocatalytic degradation various organic pollutants activity, Appl. Surf. Sci. 455 (2018) 705–716, https://doi.org/10.1016/j.apsusc.2018.06.038.

[23] S.K. Mandal, S. Paul, S. Datta, D. Jana, Nitrogenated CQD decorated ZnO nanorods towards rapid photodegradation of rhodamine B: A combined experimental and theoretical approach, Appl. Surf. Sci. 563 (2021) 150315, https://doi.org/10.1016/j.apsusc.2021.150315.

[24] W.W. Lee, C.-S. Lu, C.-W. Chuang, Y.-J. Chen, J.-Y. Fu, C.-W. Siao, C.-C. Chen, Synthesis of bismuth oxyiodides and their composites: Characterization, photocatalytic activity, and degradation mechanisms, RSC Adv. 5 (30) (2015) 23450–23463, https://doi.org/10.1039/C4RA15072D.

[25] M. Yadav, S. Garg, A. Chandra, R. Gläser, K. Hernadi, Green BiOI impregnated 2-dimensional cylindrical carbon block: A promising solution for environmental remediation and easy recovery of the photocatalyst, Sep. Purif. Technol. 240 (2020) 116628, https://doi.org/10.1016/j.seppur.2020.116628.

[26] A.A. Putri, S. Kato, N. Kishi, T. Soga, Study of annealing temperature effect on the photovoltaic performance of BiOI-based materials, Appl. Sci. 9 (16) (2019) 3342, https://doi.org/10.3390/app9163342.

[27] E. Bárdos, A.K. Király, Z. Pap, L. Baia, S. Garg, K. Hernádi, The effect of the synthesis temperature and duration on the morphology and photocatalytic activity of BiOX (X = Cl, Br, I) materials, Appl. Surf. Sci. 479 (2019) 745–756, https://doi.org/10.1016/j.apsusc.2019.02.136.

[28] J. Xia, S. Yin, H. Li, H. Xu, Y. Yan, Q.i. Zhang, Self-assembly and enhanced photocatalytic properties of BiOI hollow microspheres via a reactable ionic liquid, Langmuir. 27 (3) (2011) 1200–1206, https://doi.org/10.1021/la104054r.

[29] R. Hao, X. Xiao, X. Zuo, J. Nan, W. Zhang, Efficient adsorption and visible-light photocatalytic degradation of tetracycline hydrochloride using mesoporous BiOI microspheres, J. Hazard. Mater. 209–210 (2012) 137–145, https://doi.org/10.1016/j.jhazmat.2012.01.006.

[30] G. Wu, Y. Zhao, Y. Li, H. Ma, J. Zhao, pH-dependent synthesis of iodine-deficient bismuth oxyiodide microstructures: Visible-light photocatalytic activity, J. Colloid Interface Sci. 510 (2018) 228–236, https://doi.org/10.1016/j.jcis.2017.09.053.

[31] Y. Wang, K. Deng, L. Zhang, Visible light photocatalysis of BiOI and its photocatalytic activity enhancement by in situ ionic liquid modification, J. Phys. Chem. C. 115 (29) (2011) 14300–14308, https://doi.org/10.1021/jp2042069.

[32] L.A. Mabuti, I.K.S. Manding, C.C. Mercado, Photovoltaic and photocatalytic properties of bismuth oxyiodide-graphene nanocomposites, RSC Adv. 8 (74) (2018) 42254–42261, https://doi.org/10.1039/C8RA07360K.

[33] A.A. Putri, S. Kato, N. Kishi, T. Soga, TiO2/Bi5O7I Composite Films for Dye-Sensitized Solar Cells, J. Electron. Mater. 49 (3) (2020) 1827–1834, https://doi.org/10.1007/s11664-019-07868-2.

[34] X. Wang, C. Zhou, L. Yin, R. Zhang, G. Liu, Iodine-Deficient BiOI Nanosheets with Lowered Valence Band Maximum to Enable Visible Light Photocatalytic Activity, ACS Sustain. Chem. Eng. 7 (8) (2019) 7900–7907, https://doi.org/10.1021/acssuschemeng.9b0054810.1021/acssuschemeng.9b00548.s001.

[35] Y. Bai, T. Chen, P. Wang, L. Wang, L. Ye, Bismuth-rich Bi4O5X2 (X = Br, and I) nanosheets with dominant 1 0 1 facets exposure for photocatalytic H2 evolution, Chem. Eng. J. 304 (2016) 454–460, https://doi.org/10.1016/j.cej.2016.06.100.

[36] P. Praveenkumar, G.D. Venkatasubbu, P. Thangadurai, T. Prakash, Nanocrystalline bismuth oxyiodides thick films for X-ray detector, Mater. Sci. Semicond. Process. 104 (2019) 104686, https://doi.org/10.1016/j.mssp.2019.104686.

[37] J. You, Y. Guo, R. Guo, X. Liu, A review of visible light-active photocatalysts for water disinfection: Features and prospects, Chem. Eng. J. 373 (2019) 624–641, https://doi.org/10.1016/j.cej.2019.05.071.

[38] B. Réti, Z. Major, D. Szarka, E. Horváth, A. Magrez, L. Forró, A. Dombi, K. Hernádi, Influence of TiO2 phase composition on the photocatalytic activity of TiO2/MWCNT composites prepared by combined sol-gel/hydrothermal method, J. Mol. Catal. A Chem. 414 (2016) 140–147, https://doi.org/10.1016/j.molcata.2016.01.016.

[39] N. Syed, J. Huang, Y. Feng, X. Wang, L. Cao, Carbon-Based Nanomaterials via Heterojunction Serving as Photocatalyst, Front. Chem. 7 (2019) 1–7, https://doi.org/10.3389/fchem.2019.00713.

[40] S. Li, S. Hu, K. Xu, W. Jiang, J. Liu, Z. Wang, A novel heterostructure of BiOI nanosheets anchored onto MWCNTs with excellent visible-light photocatalytic activity, Nanomaterials. 7 (2017) 1–13, https://doi.org/10.3390/nano7010022.

[41] M. Wongaree, S. Chiarakorn, S. Chuangchote, Photocatalytic Improvement under Visible Light in TiO2 Nanoparticles by Carbon Nanotube Incorporation, J. Nanomater. 2015 (2015), https://doi.org/10.1155/2015/689306.

[42] T. A., The Role of Carbon Nanotubes in Enhancement of Photocatalysis, Synth. Appl. Carbon Nanotub. Their Compos. (2013). https://doi.org/10.5772/51050.

[43] Nikita Sharma, Zsolt Pap, Seema Garg, Klára Hernádi, Hydrothermal synthesis of BiOBr and BiOBr/CNT composites, their photocatalytic activity and the importance of early Bi6O6(OH)3(NO3)3·1.5H2O formation, Appl. Surf. Sci. 495 (2019) 143536, https://doi.org/10.1016/j.apsusc.2019.143536.

[44] Krisztina Vajda, Karoly Mogyorosi, Zoltan Nemeth, Klara Hernadi, Laszlo Forro, Arnaud Magrez, Andras Dombi, Photocatalytic activity of Tio 2/SWCNT and Tio 2/MWCNT nanocomposites with different carbon nanotube content, Phys. Status Solidi Basic Res. 248 (11) (2011) 2496–2499, https://doi.org/10.1002/pssb:v248.1110.1002/pssb:201100117.

[45] B. Réti, K. Mogyorósi, A. Dombi, K. Hernádi, Substrate dependent photocatalytic performance of TiO2/MWCNT photocatalysts, Appl. Catal. A Gen. 469 (2014) 153–158, https://doi.org/10.1016/j.apcata.2013.10.001.

[46] M. Su, C. He, L. Zhu, Z. Sun, C. Shan, Q. Zhang, D. Shu, R. Qiu, Y. Xiong, Enhanced adsorption and photocatalytic activity of BiOI-MWCNT composites towards organic pollutants in aqueous solution, J. Hazard. Mater. 229–230 (2012) 72–82, https://doi.org/10.1016/j.jhazmat.2012.05.061.

[47] Uwe Holzwarth, Neil Gibson, The Scherrer equation versus the "Debye-Scherrer equation", Nat. Nanotechnol. 6 (9) (2011) 534, https://doi.org/10.1038/nnano.2011.145.

[48] Qishe Yan, Yalei Zhao, Mengmeng Xu, Yanyan Wang, Enhanced visible-light photocatalytic performance of various bismuth oxyiode with 3D hierarchical microspheres architecture, J. Nanosci. Nanotechnol. 16 (7) (2016) 7731–7737, https://doi.org/10.1166/jnn.2016.12585.

[49] Xi Zhang, Lizhi Zhang, Electronic and band structure tuning of ternary semiconductor photocatalysts by self doping: The case of BiOI, J. Phys. Chem. C. 114 (42) (2010) 18198–18206, https://doi.org/10.1021/jp105118m.

[50] M.M. Xu, Y. Zhao, Q. Yan, Efficient visible-light photocatalytic degradation of sulfadiazine sodium with hierarchical Bi7O9I3 under solar irradiation, Water Sci. Technol. 72 (2015) 2122–2131, https://doi.org/10.2166/wst.2015.433.

[51] Changlin Yu, Caifeng Fan, Jimmy C. Yu, Wanqin Zhou, Kai Yang, Preparation of bismuth oxyiodides and oxides and their photooxidation characteristic under visible/UV light irradiation, Mater. Res. Bull. 46 (1) (2011) 140–146, https://doi.org/10.1016/j.materresbull.2010.08.013.

[52] X. Xiao, C. Xing, G. He, X. Zuo, J. Nan, L. Wang, Solvothermal synthesis of novel hierarchical Bi4O5I2 nanoflakes with highly visible light photocatalytic performance for the degradation of 4-tert-butylphenol, Appl. Catal. B Environ. 148–149 (2014) 154–163, https://doi.org/10.1016/j.apcatb.2013.10.055.

[53] Hang Liu, Jian Cai, Man Luo, Chang Chen, Pei Hu, Novel mesoporous bismuth oxyiodide single-crystal nanosheets with enhanced catalytic activity, RSC Adv. 10 (10) (2020) 5913–5918, https://doi.org/10.1039/C9RA10451H.

[54] M. Montero-Muñoz, J.E. Ramos-Ibarra, J.E. Rodríguez-Páez, M.D. Teodoro, G. E. Marques, A.R. Sanabria, P.C. Cajas, C.A. Páez, B. Heinrichs, J.A.H. Coaquira, Role of defects on the enhancement of the photocatalytic response of ZnO nanostructures, Appl. Surf. Sci. 448 (2018) 646–654, https://doi.org/10.1016/j.apsusc.2018.04.105.

[55] Daimei Chen, Zhihong Wang, Tiezhen Ren, Hao Ding, Wenqing Yao, Ruilong Zong, Yongfa Zhu, Influence of defects on the photocatalytic activity of ZnO, J. Phys. Chem. C. 118 (28) (2014) 15300–15307, https://doi.org/10.1021/jp5033349.

[56] Dileep Maarisetty, Saroj Sundar Baral, Defect engineering in photocatalysis: formation, chemistry, optoelectronics, and interface studies, J. Mater. Chem. A. 8 (36) (2020) 18560–18604, https://doi.org/10.1039/D0TA04297H.

[57] J. Yang, L. Xu, C. Liu, T. Xie, Preparation and photocatalytic activity of porous Bi5O7I nanosheets, Appl. Surf. Sci. 319 (2014) 265–271, https://doi.org/10.1016/j.apsusc.2014.07.055.

[58] M. Ashraf, M. Yusoff, S.S. Imam, I. Shah, Photocatalytic activity of bismuth oxyiodide nanospheres and nanoplates in the degradation of ciprofloxacin under visible light Photocatalytic activity of bismuth oxyiodide nanospheres and nanoplates in the degradation of cipro fl oxacin under visible lig, (2019).

[59] Chao Liu, Xiao-jing Wang, Room temperature synthesis of Bi4O5I2 and Bi5O7I ultrathin nanosheets with a high visible light photocatalytic performance, Dalt. Trans. 45 (18) (2016) 7720–7727, https://doi.org/10.1039/C6DT00530F.

[60] J.A. Steele, R.A. Lewis, Laser-induced oxidation kinetics of bismuth surface microdroplets on GaAsBi studied in situ by Raman microprobe analysis, Opt. Express. 22 (26) (2014) 32261, https://doi.org/10.1364/OE.22.032261.

[61] Bei Long, Yongchao Huang, Haibo Li, Fengyi Zhao, Zebao Rui, Zili Liu, Yexiang Tong, Hongbing Ji, Carbon Dots Sensitized BiOI with Dominant 001 Facets for Superior Photocatalytic Performance, Ind. Eng. Chem. Res. 54 (51) (2015) 12788–12794, https://doi.org/10.1021/acs.iecr.5b02780.

[62] Siwen Gong, Gangqiang Zhu, Isaac Asusheyi Bello, Fei Rao, Shiping Li, Jianzhi Gao, Siyaka Mj Zubairu, Jianhong Peng, Mirabbos Hojamberdiev, Constructing 1D/2D BiOI/ZnWO4 p-n heterojunction photocatalyst with enhanced photocatalytic removal of NO, J. Chem. Technol. Biotechnol. 95 (6) (2020) 1705–1716, https://doi.org/10.1002/jctb.v95.610.1002/jctb.6368.

[63] Alexander A. Kharlamov, Rui M. Almeida, Jong Heo, Vibrational spectra and structure of heavy metal oxide glasses, J. Non. Cryst. Solids. 202 (3) (1996) 233–240, https://doi.org/10.1016/0022-3093(96)00192-5.

[64] Franklin D. Hardcastle, Israel E. Wachs, The molecular structure of bismuth oxide by Raman spectroscopy, J. Solid State Chem. 97 (2) (1992) 319–331, https://doi.org/10.1016/0022-4596(92)90040-3.

[65] Hongwei Huang, Xiaowei Li, Xu Han, Na Tian, Yihe Zhang, Tierui Zhang, Moderate band-gap-broadening induced high separation of electron-hole pairs in Br substituted BiOI: A combined experimental and theoretical investigation, Phys. Chem. Chem. Phys. 17 (5) (2015) 3673–3679, https://doi.org/10.1039/C4CP04842C.

[66] J. Han, G. Zhu, M. Hojamberdiev, J. Peng, X. Zhang, Y. Liu, B. Ge, P. Liu, Rapid adsorption and photocatalytic activity for Rhodamine B and Cr(VI) by ultrathin BiOI nanosheets with highly exposed 001 facets, New J. Chem. 39 (2015) 1874–1882, https://doi.org/10.1039/c4nj01765j.

[67] Yohan Park, Yulyi Na, Debabrata Pradhan, Bong-Ki Min, Youngku Sohn, Adsorption and UV/Visible photocatalytic performance of BiOI for methyl orange, Rhodamine B and methylene blue: Ag and Ti-loading effects, CrystEngComm. 16 (15) (2014) 3155–3167, https://doi.org/10.1039/C3CE42654H.